LONGITUDINAL MATCHING AND TIMING CONTROL STUDIES FOR THE PERLE ENERGY RECOVERY LINAC

J. Issa*, A. Fomin, J. Michaud, Université Paris-Saclay, CNRS/IN2P3, IJCLab, Orsay, France
F. Bouly, Laboratoire de Physique Subatomique et de Cosmologie, Grenoble, France

Abstract

In an Energy Recovery Linac (ERL), precise longitudinal dynamics control is essential for both delivering the required bunch parameters at the interaction points and for enabling energy recovery. This paper will specifically talk about these studies for the PERLE accelerator. PERLE (Powerful Energy Recovery Linac for Experiments) is a proposed high-power ERL delivering a 250 MeV, 20 mA beam (5 MW). Its multi-pass lattice combines the energy of circular machines with the beam quality of a linac, but also inherits their main limitations. In particular, this paper will present studies done of longitudinal matching, this means setting the right correlation between the particle's longitudinal position and its energy, as well as developing a chicane for timing control.

INTRODUCTION

PERLE (Powerful Energy Recovery Linac for Experiments) is a high-current ERL designed to deliver an electron beam of up to 250 MeV in its first phase [1]. Its multi-pass layout combines the beam quality of a linac with recirculation; however, it also inherits strong sensitivity to longitudinal dynamics, timing, and nonlinear effects.

In such a machine, the beam passes several times through the same RF cavities. Any mismatch in longitudinal phase space is, therefore, transported through the machine and can accumulate over multiple passes. A correct longitudinal match is required not only to reach the desired beam conditions at the interaction points but also to ensure proper beam transport and efficient energy recovery.

The longitudinal motion is described in terms of the particle position z (or time t) with respect to the reference particle and the relative energy deviation δ. The evolution of the longitudinal coordinate can be written as [2]

$$z_f = z_i + R_{56}\,\delta + T_{566}\,\delta^2 + U_{5666}\,\delta^3 + O(\delta^4), \qquad (1)$$

where R_{56} is the first-order longitudinal dispersion and T_{566} is the second-order longitudinal term.

The term R_{56} represents the linear dependence of path length on energy. In dispersive regions, particles with different δ follow different trajectories, which leads to a shift in arrival time. This is the main quantity used to manipulate the longitudinal phase space. In practice, R_{56} can be tuned through the optics of dispersive sections, typically in the arcs, or the merger if the design includes a quadrupole to allow it (such as the merger design of PERLE). By adjusting quadrupole strengths, the dispersion function is modified, which directly changes the value of R_{56}.

* issa@ijclab.in2p3.fr

This is combined with off-crest acceleration, which introduces a correlation between z and δ (chirp). The combination of chirp and R_{56} allows a rotation of the longitudinal phase space, which can be used either to compress the bunch or to reduce the energy spread, depending on the chosen configuration.

The present work focuses on two aspects. The first is longitudinal matching at specific locations of the machine. The second is timing control and synchronization through a magnetic chicane introduced to vary the path length and, therefore, the arrival phase (i.e. time) of the recirculating beam without changing the RF cavity phases.

METHODOLOGY

The studies were carried out for the one-turn version of PERLE using Bmad/Tao with absolute time-domain tracking [3]. Compared with more traditional s-domain tracking, this makes it possible to directly follow particle arrival times and, therefore, treat timing constraints more realistically.

The longitudinal matching follows from the fact that R_{56} has no effect without an initial chirp. Hence, a chirped initial distribution is first used, as obtained from injector simulations [4]. The longitudinal phase space is then shaped progressively by tuning R_{56} in the merger, further chirped by introducing off-crest acceleration, and then tuning R_{56} in the arcs. During deceleration, the chicane is used to recover the correct arrival phase and, therefore, achieve more efficient energy recovery [5].

At the interaction points, both bunch-length minimization and energy-spread minimization are studied to determine the range within which the machine can operate and to address future experimental requirements. At the end of the machine, the study is performed after deceleration and is used as a benchmark for the future three-turn machine.

The machine layout and the locations considered in this study are shown in Fig. 1.

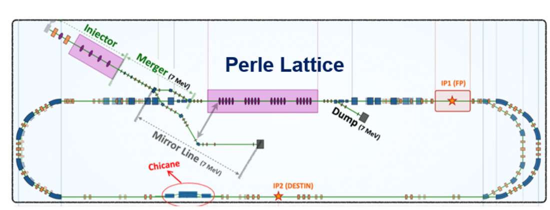

Figure 1: PERLE layout showing the injector, common section, recirculation arcs, and the interaction points considered for longitudinal matching.

CHICANE MODEL FOR TIMING CONTROL

In ERL, the RF cavity phases are fixed during operation, so timing adjustments must be made through the beamline itself. For this reason, a magnetic chicane was studied in order to modify the path length and, therefore, the recirculating beam arrival phase in the cavities. The corresponding three-dipole geometry is shown in Fig. 2.

The chosen geometry is a symmetric three-dipole chicane. The two outer dipoles have a length L_1 and bend the beam by an angle θ, while the central dipole has a length $2L_1$ and bends by -2θ. This ensures that the trajectory returns to the same line as the input one while changing the total path length.

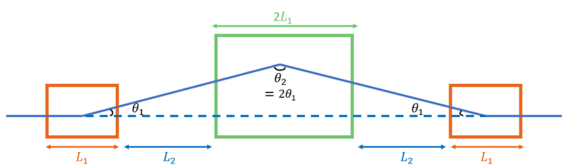

Figure 2: Three-dipole chicane geometry used for timing control.

The bending angle of each dipole depends on the magnetic field as

$$\theta(B) = \frac{qBL_1}{p}, \tag{2}$$

where q is the particle charge and p its momentum.

The path length in the chicane insertion is written as

$$S(B) = 4\frac{L_1}{\sin\theta(B)}\theta(B) + 2\frac{L_2}{\cos\theta(B)}, \tag{3}$$

where L_2 is the drift length between the dipoles.

The corresponding RF phase shift is then

$$\Delta\phi = \frac{\omega_{\mathrm{RF}}}{c}\left[S(B) - S(B_0)\right], \tag{4}$$

where B_0 is the nominal dipole field. Here, B_0 corresponds to the reference trajectory for which the beam returns with zero RF phase shift after one turn in the machine, i.e. no additional arrival phase with respect to the cavities. The quantity used in the optimization is the variation of the magnetic field around this value.

CHICANE VALIDATION

The effect of the chicane on the beam arrival phase was studied both analytically and using Bmad time-tracking, as shown in Fig. 3.

The phase shift varies linearly with the field shift over the studied range. The analytical model and the tracking results are in agreement, which validates the analytical description of the chicane.

The slope of the curve shows that small variations in the dipole field, on the order of mT, are sufficient to produce the required phase correction.

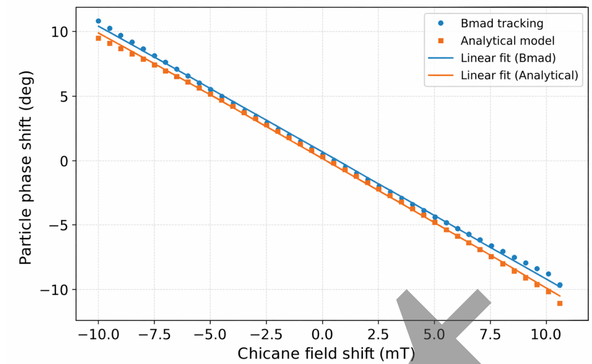

Figure 3: RF phase shift as a function of chicane field shift around the reference field B_0: analytical model and Bmad tracking.

LONGITUDINAL MATCHING RESULTS AND ANALYSIS

Interaction Points

The two interaction points are located at different stages of the machine and therefore do not offer the same longitudinal tuning capabilities.

IP1 is reached after a single accelerating pass, directly after the injector and the first linac. At this stage, the beam has not yet passed through any recirculation arc. This limits the available control over the longitudinal distribution, so the achievable optimization remains constrained, and reaching the target beam conditions can more easily lead to downstream losses.

IP2 is located further downstream, after additional transport through dispersive sections. While this provides more flexibility to shape the longitudinal phase space, the matching remains limited by the fact that the beam has still experienced only one accelerating passage through the linac. As a result, the achievable compression and energy-spread reduction remain moderate at both interaction points.

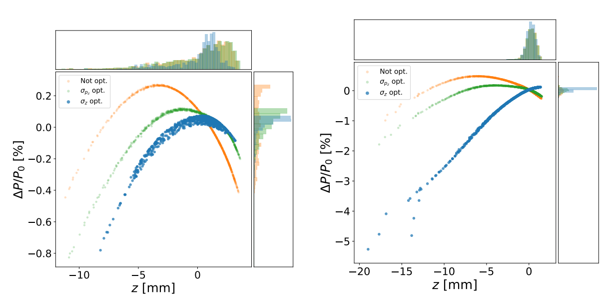

(a) (b)

Figure 4: Longitudinal phase space at the interaction points: (a) IP1 and (b) IP2. In both cases, the orange distribution corresponds to the base configuration without matching, the blue distribution to the bunch-length optimization case, and the green distribution to the energy-spread optimization case. The side histograms represent the corresponding projections in z and δ.

At IP1, shown in Fig. 4a, the bunch length is reduced from 2.89 mm to 2.13 mm (about 26%) with moderate losses. In a separate setting, the energy spread is reduced from 0.2% to 0.17% (about 15%). The remaining curvature is due to RF nonlinearities.

At IP2, shown in Fig. 4b, the bunch length is reduced from 3 mm to 2.73 mm (about 9%), with negligible losses. The energy spread, tuned in a separate study is reduced from 0.2% to 0.17% (about 15%).

End of the Machine

The optimized longitudinal phase space after deceleration at the cryomodule exit is shown in Fig. 5.

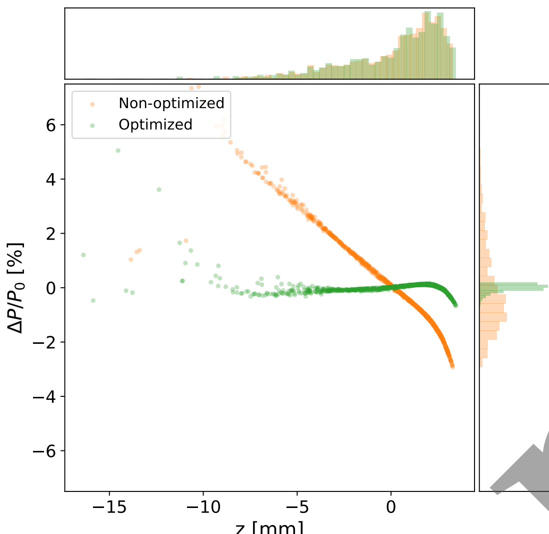

Figure 5: Longitudinal phase space at the cryomodule exit after deceleration. The orange distribution corresponds to the base configuration without matching, while the green distribution shows the optimized case with reduced energy spread. The side histograms represent the corresponding projections in z and δ.

After deceleration, the energy spread is reduced from 1.87% to 0.26% (about 86%). The phase-space distribution shows a flattening of the energy profile.

The corresponding parameters used for the different configurations are summarized in Table 1.

DISCUSSION AND CONCLUSION

The results show that the achievable longitudinal matching depends on the location in the machine. At IP1, the beam has only undergone a single accelerating pass through the linac, which limits the effect of R_{56} and constrains the achievable optimization. At IP2, the additional transport helps shaping the longitudinal phase space, even if the matching is still limited by the single-pass configuration.

In addition, after deceleration, when the beam passes through the linac a second time, it enables stronger control of energy spread. This shows that efficient energy spread minimization requires at least two passages through the linac,

Table 1: The phase ϕ_{cav} is the global phase offset applied to the linac (equivalent model for the 4 cavities of the ERL cryomodule) with respect to the on-crest condition ($\phi_{\text{cav}} = 0$). B_{shift} is the variation of the chicane magnetic field with respect to its reference value. R_{56}^{merg} and R_{56}^{arc} correspond to the longitudinal dispersion in the merger and in the recirculation arc, respectively.

Case	ϕ_{cav} (°)	B_{shift} (mT)	R_{56}^{merg} (m)	R_{56}^{arc} (m)
IP1, σ_z opt.	1.8	1.0	-0.48125	—
IP1, σ_{p_z} opt.	5.76	1.0	0.0158	—
IP2, σ_z opt.	9.72	-1.0	0.0095	0.000215
IP2, σ_{p_z} opt.	5.76	1.0	0.0158	-0.001098
End, σ_{p_z} opt.	-14.76	0.17	—	—

which is why this configuration is mainly used here as a benchmark for the future three-turn machine.

Overall, the one-turn configuration of PERLE already gives good results for longitudinal matching, while also showing the improvement expected with additional passes. This makes the extension to three turns very promising, with the chicane providing the required synchronicity control for energy recuperation, without modifying the RF settings.

Future work focuses on the three-turn machine. With multiple passes through the linac, the longitudinal phase space can be further shaped from pass to pass, reaching conditions that were not accessible in the one-turn case. This also introduces additional constraints, since the beam loading must remain consistent over all passes. In addition, sextupoles will be introduced to control higher-order terms, in particular T_{566}, to correct the remaining second-order curvature.

REFERENCES

[1] S. A. Bogacz *et al.*, "Beam dynamics driven design of powerful energy recovery linac for experiments", *Phys. Rev. Accel. Beams*, vol. 27, p. 031603, 2024. doi:10.1103/PhysRevAccelBeams.27.031603

[2] G. Pérez Segurana, "Longitudinal beam dynamics and longitudinal matches in energy recovery linacs", Ph.D. thesis, Lancaster University, 2022. doi:10.17635/lancaster/thesis/1651

[3] D. Sagan, "Bmad: a relativistic charged particle simulation library", *Nucl. Instrum. Methods Phys. Res., Sect. A*, vol. 558, no. 1, pp. 356–359, 2006. doi:10.1016/j.nima.2005.11.001

[4] C. K. Monaghan and C. P. Welsch, "Optimisation of the perle injector using a multi-objective genetic algorithm", in *Proc. IPAC'24*, Nashville, TN, USA, pp. 2022–2025, May 2024. doi:10.18429/JACoW-IPAC2024-WEPC25

[5] J. Michaud *et al.*, "Status of the beam dynamics studies for the perle energy recovery linac", in *Proc. IPAC'25*, Taipei, Taiwan, pp. 702–705, Jun. 2025. doi:10.18429/JACoW-IPAC2025-MOPS041